Entropy optimization in Darcy–Forchheimer MHD flow of water based copper and silver nanofluids with Joule heating and viscous dissipation effects

Zahir Shah, Luthais B. McCash, Abdullah Dawar, et al.

View Online   Export Citation   CrossMark

ARTICLES YOU MAY BE INTERESTED IN

Call For Papers!

AIP Advances

SPECIAL TOPIC: Advances in Low Dimensional and 2D Materials

Entropy optimization in Darcy–Forchheimer MHD flow of water based copper and silver nanofluids with Joule heating and viscous dissipation effects

Zahir Shah,[1] (ID) Luthais B. McCash,[2] (ID) Abdullah Dawar,[3] (ID) and Ebenezer Bonyah[4,a)] (ID)

AFFILIATIONS

[1] Center of Excellence in Theoretical and Computational Science (TaCS-CoE), SCL 802 Fixed Point Laboratory, Science Laboratory Building, King Mongkut's University of Technology Thonburi (KMUTT), 126 Pracha-Uthit Road, Bang Mod, Thrung Khru, Bangkok 10140, Thailand

[2] Department of Mathematics, College of Science and Engineering University of Leicester, University Road, Leicester LE1 7RH, United Kingdom

[3] Department of Mathematics, Abdul Wali Khan University, Mardan 23200, KPK, Pakistan

[4] Department of Mathematics Education, University of Education, Winneba Kumasi-(Kumasi Campus), Winneba 00233, Ghana

a)Author to whom correspondence should be addressed: ebbonya@gmail.com

ABSTRACT

The irreversibility examination in steady flows of water based silver and copper nanofluids between two rotating disks is presented in this paper. The Darcy–Forchheimer relation is applied to the fluid flow. The two disks are kept at constant temperatures and are rotating with angular velocities. A magnetic field along radial and tangential directions is also applied. Moreover, viscous dissipation, heat generation, and Joule heating influences are taken in the nanofluid flows. The modeled problem is treated with the homotopy analysis method (HAM) and shooting techniques. The deviations in both nanofluids due to embedded factors are shown in graphs. The HAM and shooting techniques are compared and are shown with the help of figures and tables. The leading arguments of the current study are stated in the concluding section.

I. INTRODUCTION

At present, nanofluid analysis is a prevalent area of research. A suspension of solid nanoparticles in a base fluid is called a nanofluid. Such fluids have much greater ability of thermal conduction as compared to pure base fluids. The applications of nanofluids in the field of medicine include nanodrugs, electromechanical systems, optical sensors, cooling and heating devices, etc. Initially, Choi[1] observed the enhancement in fluid thermal conductivity by using nanoparticles. To analyze the thermal transfer characteristics of fluids, Hwang et al.[2] analyzed Al_2O_3 nanoparticles in water based nanofluids. Bhatti and Rashidi[3] investigated the

Williamson fluid flow over a stretched surface. The numerical analysis of nanofluid flows through porous walls was examined by Hatami et al.[4] The analysis of radiative water based copper and silver nanofluids was probed by Hayat et al.[5] The peristaltic flows of copper oxide water based nanofluids in a porous tube were presented by Akbar et al.[6] The nanofluid flow with shape effects of nanoparticles and entropy optimization was discussed by Ellahi et al.[7] Nanofluids with magnetic field influence are magneto-nanofluids. Drug targeting, magnetohydrodynamic (MHD) sensors, nuclear reactors, power generators, plasma confinement and accelerators, etc., are the applications of MHD. The magnetic field influence on convective three-dimensional (3D) nanofluids was studied by Sheikholeslami and

Ellahi.[8] Hayat *et al.*[9] presented the magnetohydrodynamic nanofluid flow through an extending surface. Abbasi *et al.*[10] presented the convective Maxwell nanofluid flow with a heat source/sink. The flow of unsteady MHD nanofluids over a rotating cone was presented by Raju *et al.*[11] The thermal and mass transmission in chemically reactive MHD nanofluids was analyzed by Jonnadula *et al.*[12] Ellahi[13] probed the MHD nanofluid with thermal dependent viscosity. The magnetohydrodynamic flow of nanofluids with radiation influence was presented by Kumam *et al.*[14] The MHD radiative Eyring–Powell fluid flow was investigated by Alharbi *et al.*[15] Khan *et al.*[16] inspected the MHD Forchheimer nanofluid flow in the rotating frame. The MHD fluid flow with Hall current was investigated by Shah *et al.*[17]

The researchers have shown much interest in the fluid flows by two rotating disks. The convenient applications are in aircrafts, gas turbines, car bake systems, engines, atomizers, computer disk drives, medical equipment, rotational air cleaners, evaporators, and extractors. Turkyilmazoglu[18] investigated the boundary layer flow in a rotating disk. Hatami *et al.*[19] explored the thermal characteristics of nanofluids in rotating disks. Yan and Soong[20] analyzed the convective flows in rotating disks. You *et al.*[21] numerically investigated elastic–plastic rotating disks. Soong[22] theoretically investigated the mixed convective flows in rotating disks. Hayat *et al.*[23] presented the fluid flow with chemical reactions by a rotating disk. Alreshidi *et al.*[24] investigated the nanofluid flow with Joule heating considering slip conditions by a rotating disk.

In order to verify the recital of numerous systems used in engineering and industrial applications, entropy optimization is used. Therefore, many engineers and researchers have struggled with the problems of entropy generation. Initially, Bejan[25] presented the theoretical analysis on entropy optimization. The irreversibility examination in MHD flows of the Newtonian fluid over an extending disk was probed by Hayat *et al.*[26] Dawar *et al.*[27] probed the irreversibility in MHD flows of the nanofluid. The irreversibility examination in a viscous fluid over an extending sheet was scrutinized by Govindaraju *et al.*[28] The Newtonian convective fluid flow with the irreversibility process was presented by Khan *et al.*[29] The irreversibility analysis in the radiative Newtonian fluid with the buoyancy force was presented by Ganesh *et al.*[30] Some further studies related to entropy optimization can be seen in Refs. 31–35. Numerical and analytical studies of the boundary value problem with different approaches and effects can be seen in Refs. 36–39.

In view of the above-mentioned literature survey, the entropy generation in MHD flows of water based silver and copper nanofluids is presented in this work. The nanofluid flows are taken between two stretched rotating disks. A porous medium is filled by incompressible fluids that are categorized by the Darcy–Forchheimer relation.

II. PROBLEM FORMULATION

The axisymmetric flows of water based silver and copper nanofluids between two rotating disks are assumed here. The two lower and upper disks are located at $z = 0$ and $z = h$, respectively (Fig. 1). T_1 and T_2 are considered the two constant temperatures at lower and upper disks correspondingly. The disks are rotating with angular velocities γ_1 and γ_2 with stretching rates λ_1 and λ_2, respectively. The copper and silver water based nanofluids contain
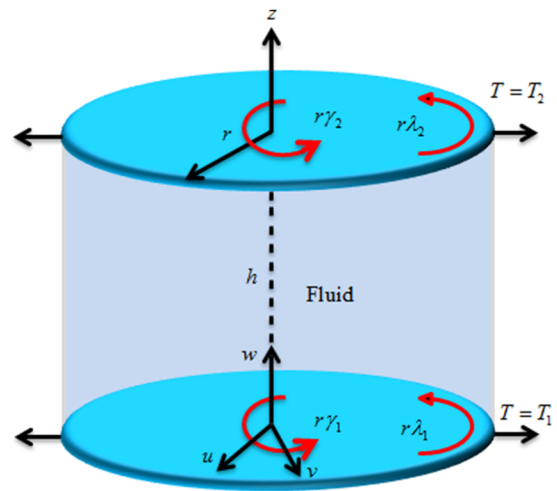

FIG. 1. Flow geometry.

nanoparticles. A porous medium is filled by incompressible fluids that are categorized by the Darcy–Forchheimer relation. A magnetic field along radial and tangential directions is applied. Moreover, heat generation, Joule heating, and viscous dissipation are presented. In the presence of silver and copper (base fluids) nanofluids, entropy optimization is investigated. The principal equations for the contemporary flow with cylindrical coordinates are[40]

$$\frac{\partial u}{\partial r} + \frac{\partial w}{\partial z} + \frac{u}{r} = 0, \tag{1}$$

$$u\frac{\partial u}{\partial r} + w\frac{\partial u}{\partial z} - \frac{v^2}{r} = v_{nf}\left(\frac{\partial^2 u}{\partial r^2} - \frac{u}{r^2} + \frac{\partial^2 u}{\partial z^2} + \frac{1}{r}\frac{\partial u}{\partial r}\right) - \frac{\sigma_{nf}B_0^2}{\rho_{nf}}u$$
$$- \frac{v_{nf}u}{K} - \frac{F^* u^2}{K^{1/2}}, \tag{2}$$

$$u\frac{\partial v}{\partial r} + w\frac{\partial v}{\partial z} - \frac{uv}{r} = v_{nf}\left(\frac{\partial^2 v}{\partial r^2} - \frac{v}{r^2} + \frac{\partial^2 v}{\partial z^2} + \frac{1}{r}\frac{\partial v}{\partial r}\right) - \frac{\sigma_{nf}B_0^2}{\rho_{nf}}v, \tag{3}$$

$$u\frac{\partial w}{\partial r} + w\frac{\partial w}{\partial z} = v_{nf}\left(\frac{\partial^2 w}{\partial z^2} + \frac{1}{r}\frac{\partial w}{\partial r} + \frac{\partial^2 w}{\partial r^2}\right) - \frac{v_{nf}w}{K} - \frac{F^* w^2}{K^{1/2}}, \tag{4}$$

$$(\rho c_p)_{nf}\left(w\frac{\partial T}{\partial z} + u\frac{\partial T}{\partial r}\right) = k_{nf}\left(\frac{1}{r}\frac{\partial T}{\partial r} + \frac{\partial^2 T}{\partial z^2} + \frac{\partial^2 T}{\partial r^2}\right)$$
$$+ \sigma_{nf}B_0^2\left(u^2 + v^2\right) + Q_0(T - T_2)$$
$$+ \mu_{nf}\left[2\left(\frac{\partial u}{\partial r}\right)^2 + \frac{2}{r^2}u^2 + 2\left(\frac{\partial w}{\partial z}\right)^2 + \left(\frac{\partial v}{\partial z}\right)^2\right.$$
$$\left. + \left(\frac{\partial w}{\partial r} + \frac{\partial u}{\partial z}\right)^2 + r\frac{\partial}{\partial r}\left(\frac{v}{r}\right)^2\right]. \tag{5}$$

The conditions at the boundaries are

$$u = \lambda_1 r, \ v = \gamma_1 r, \ w = 0, \ T = T_1 \text{ at } z = 0, \ u = \lambda_2 r,$$
$$v = \gamma_2 r, \ w = 0, \ T = T_2 \text{ at } z = h. \tag{6}$$

The fundamental properties of the nanofluid are[41–44]

$$\frac{\mu_{nf}}{\mu_f} = \frac{1}{(1-\varphi)^{2.5}}, \quad \rho_{nf} = \varphi\rho_s + (1-\varphi)\rho_f,$$

$$(\rho c_p)_{nf} = (1-\varphi)(\rho c_p)_f + \varphi(\rho c_p)_s,$$

$$\frac{\sigma_{nf}}{\sigma_f} = \frac{3\varphi\left(\frac{\sigma_s}{\sigma_f}-1\right)}{\left(\frac{\sigma_s}{\sigma_f}+2\right) - \varphi\left(\frac{\sigma_s}{\sigma_f}-1\right)} + 1, \quad \frac{k_{nf}}{k_f} = \frac{(k_s+2k_f) - 2\varphi(k_f-k_s)}{(k_s+2k_f) + \varphi(k_f-k_s)}. \tag{7}$$

In the above equations, u, v, and w are the velocity components along $r-$, $\theta-$, and $z-$ directions, respectively, T_1 and T_2 are the temperatures of lower and upper disks, respectively, Q_0 is the heat generation, F^* and K are the Forchheimer coefficient and porous medium permeability, μ_{nf} is the dynamic viscosity, v_{nf} is the kinematic viscosity, k_{nf} is the thermal conductivity, ρ_{nf} is the density, σ_{nf} is the electrical conductivity, $(\rho c_p)_{nf}$ is the capacitance of the nanofluid, φ is the nanoparticle volume fraction, and the subscripts nf, s, and f are used for thermo-physical properties of the nanofluid, nano-solid particles, and base fluid, respectively.

The following transformations are defined:

$$u = \gamma_1 r f'(\omega), \quad v = \gamma_1 r g(\omega), \quad w = -2h\gamma_1 f(\omega),$$

$$\theta(\omega) = \frac{T-T_2}{T_1-T_2}, \quad \omega = \frac{z}{h}. \tag{8}$$

Using Eq. (8), Eq. (1) is obvious and Eqs. (2)–(6) are reduced as

$$\frac{1}{(1-\varphi)^{2.5}\left(1-\varphi+\frac{\rho_s}{\rho_f}\varphi\right)}f''' + 2\mathrm{Re}ff'' - \mathrm{Re}f'^2 + \mathrm{Re}g^2$$

$$- \frac{\sigma_{nf}}{\sigma_f}\frac{\mathrm{Re}Ha}{\left(1-\varphi+\frac{\rho_s}{\rho_f}\varphi\right)}f' - \frac{\mathrm{Re}\lambda}{(1-\varphi)^{2.5}\left(1-\varphi+\frac{\rho_s}{\rho_f}\varphi\right)}f'$$

$$- \mathrm{Re}Ff'^2 = 0, \tag{9}$$

$$\frac{1}{(1-\varphi)^{2.5}\left(1-\varphi+\frac{\rho_s}{\rho_f}\varphi\right)}g'' + 2\mathrm{Re}fg' - 2\mathrm{Re}gf' - \mathrm{Re}f'^2$$

$$- \frac{\sigma_{nf}}{\sigma_f}\frac{\mathrm{Re}Ha}{\left(1-\varphi+\frac{\rho_s}{\rho_f}\varphi\right)}g = 0, \tag{10}$$

$$\frac{2}{(1-\varphi)^{2.5}\left(1-\varphi+\frac{\rho_s}{\rho_f}\varphi\right)}f'' - \frac{2\mathrm{Re}\lambda}{(1-\varphi)^{2.5}\left(1-\varphi+\frac{\rho_s}{\rho_f}\varphi\right)}f$$

$$+ 4\mathrm{Re}ff' + 4\mathrm{Re}Ff^2 = 0, \tag{11}$$

$$\frac{(k_s+2k_f) - 2\varphi(k_f-k_s)}{(k_s+2k_f) + \varphi(k_f-k_s)}\theta'' + \frac{2\mathrm{Re}Pr}{\left(1-\varphi+\frac{(\rho c_p)_s}{(\rho c_p)_f}\varphi\right)}f\theta'$$

$$+ \frac{Br}{(1-\varphi)^{2.5}}\left(f''^2 + g'^2 + \frac{12}{A}f'^2\right) + \mathrm{Re}MBr\left(f'^2+g^2\right)$$

$$+ \mathrm{Re}Pr\beta\theta = 0, \tag{12}$$

$$f = 0, \ f' = A_1, \ g = 1, \ \theta = 1 \text{ at } \omega = 0,$$

$$f' = A_2, \ g = \gamma, \ \theta = 0 \text{ at } \omega = 1. \tag{13}$$

Here, Re is the Reynolds number, Ha is the Hartmann number, λ is the porosity parameter, Pr is the Prandtl number, F is the local inertial coefficient, A_1 and A_2 are stretching parameters, Ec is the Eckert number, Br is the Brinkman number, β is the heat generation parameter, and γ is the rotation parameter, which are defined as

$$\mathrm{Re} = \frac{h^2\gamma_1}{v_f}, \ Ha = \frac{\sigma_f B_0^2}{\rho_f\gamma_1}, \ \lambda = \frac{v_f}{\gamma_1 K}, \ \mathrm{Pr} = \frac{v_f}{\alpha_f}, \ \beta = \frac{Q_0}{(c_p)_f\gamma_1},$$

$$F = \frac{F^* r}{K^{1/2}}, \ \gamma = \frac{\gamma_2}{\gamma_1}, \ Ec = \frac{\gamma_1^2 r^2}{c_p(T_1-T_2)}, \ A_1 = \frac{\lambda_1}{\gamma_1}, \tag{14}$$

$$A_2 = \frac{\lambda_2}{\gamma_1}, \ Br = Ec.\mathrm{Pr}.$$

III. PHYSICAL QUANTITIES OF INTEREST

The surface drag force at the lower disk (C_{f0}) and upper disk (C_{f1}) is defined as

$$C_{f0} = \frac{\tau_w|_{z=0}}{r^2\gamma_1^2\rho_f}, \ C_{f1} = \frac{\tau_w|_{z=h}}{r^2\gamma_1^2\rho_f}, \tag{15}$$

where $\tau_w = \left(\tau_{zr}^2 + \tau_{z\theta}^2\right)^{1/2}$ is the shear stress, in which τ_{zr} and $\tau_{z\theta}$ are the shear stresses at lower and upper disks, respectively, and are defined as

$$\tau_{zr} = \mu_{nf}\frac{\partial u}{\partial z}\Big|_{z=0} = \frac{\mu_f}{(1-\varphi)^{2.5}}\frac{r\gamma_1}{h}f''(0) \text{ (lower disk)},$$

$$\tau_{zr} = \mu_{nf}\frac{\partial u}{\partial z}\Big|_{z=h} = \frac{\mu_f}{(1-\varphi)^{2.5}}\frac{r\gamma_1}{h}f''(1) \text{ (upper disk)}, \tag{16}$$

$$\tau_{z\theta} = \mu_{nf}\frac{\partial v}{\partial z}\Big|_{z=0} = \frac{\mu_f}{(1-\varphi)^{2.5}}\frac{r\gamma_1}{h}g'(0) \text{ (lower disk)},$$

$$\tau_{z\theta} = \mu_{nf}\frac{\partial v}{\partial z}\Big|_{z=h} = \frac{\mu_f}{(1-\varphi)^{2.5}}\frac{r\gamma_1}{h}g'(1) \text{ (upper disk)}. \tag{17}$$

The dimensionless form of Eqs. (16) and (17) is

$$C_{f0}\mathrm{Re}_r = \frac{1}{(1-\varphi)^{2.5}}\sqrt{(g'(0))^2 + (f''(0))^2}, \tag{18}$$

$$C_{f1}\mathrm{Re}_r = \frac{1}{(1-\varphi)^{2.5}}\sqrt{(g'(1))^2 + (f''(1))^2}. \tag{19}$$

The rate of thermal transmission at lower (Nu_{x0}) and upper (Nu_{x1}) disks is stated as

$$Nu_{x0} = \frac{hq_w}{(T_1-T_2)k_f}\Big|_{z=0}, \ Nu_{x1} = \frac{hq_w}{(T_1-T_2)k_f}\Big|_{z=h}, \tag{20}$$

where $q_w = -k_{nf}\frac{\partial T}{\partial z}\big|_{z=0}$ and $q_w = -k_{nf}\frac{\partial T}{\partial z}\big|_{z=h}$ are the heat fluxes at lower and upper disks, respectively.

The dimensionless form of Eq. (20) is

$$Nu_{x0} = -\frac{k_{nf}}{k_f}\theta'(0), \ Nu_{x1} = -\frac{k_{nf}}{k_f}\theta'(1). \tag{21}$$

IV. ENTROPY GENERATION

Analyzing the second law behavior of the steady flow of water based silver and copper nanofluids between rotating disks through entropy optimization, the basic equation for entropy is written as

$$S_G = \frac{k_{nf}}{T_f^2}\left(\frac{\partial T}{\partial y}\right)^2 + \frac{\mu_{nf}}{T_f}\left\{2\left(\frac{\partial u}{\partial r}\right)^2 + \frac{2}{r}(u)^2 + 2\left(\frac{\partial w}{\partial z}\right)^2 + \left(\frac{\partial v}{\partial z}\right)^2 \right.$$
$$\left. + \left(\frac{\partial w}{\partial r} + \frac{\partial u}{\partial z}\right)^2 + r\frac{\partial}{\partial r}\left(\frac{v}{r}\right)^2\right\} + \frac{\sigma_{nf}B_0^2}{T_f}\left(u^2 + v^2\right), \qquad (22)$$

which is reduced as

The Bejan number is reduced as

$$Be = \frac{\frac{k_{nf}}{k_f}T_d\theta'^2}{\frac{k_{nf}}{k_f}T_d\theta'^2 + \frac{Br}{Re}\frac{1}{(1-\varphi)^{2.5}}\left\{A\left(g'^2 + f''^2\right) + 12f'^2\right\} + ABrHa\left(g^2 + f'^2\right)}. \qquad (25)$$

Here, N_G depicts the entropy generation rate, Br is the Brinkman number, and T_d is the temperature difference, which are defined as

$$N_G = \frac{S_G T_f \nu_f}{(T_1 - T_2)k_f}, \quad Br = \frac{\mu_f h^2 \gamma^2}{(T_1 - T_2)k_f}, \quad T_d = \frac{(T_1 - T_2)}{T_f}. \qquad (26)$$

V. METHODOLOGY

The model equations (9)–(13) are solved by using the homotopy analysis method (HAM) and shooting techniques. The HAM is a semi-analytical method that agrees with the convergence of the proposed model. The analytical solution of the modeled equations (9)–(12) with boundary conditions (13) is treated with the help of computed codes using Mathematica 10.0. The initial supposition $[f_0(\omega), g_0(\omega), \text{and } \theta_0(\omega)]$ and linear operatives (L_f, L_g, and L_θ) are stated as

$$f_0(\omega) = A_1\omega - \frac{A_1}{2}\omega^2 + A_2\omega^2, \ g_0(\omega) = 1 + (\gamma - 1)\omega, \ \theta_0(\omega) = 1 - \omega, \qquad (27)$$

$$L_f = \frac{\partial^3 f}{\partial \omega^3}, \ L_g = \frac{\partial^2 g}{\partial \omega^2}, \ L_\theta = \frac{\partial^2 \theta}{\partial \omega^2}, \qquad (28)$$

with

$$L_f = j_1 + j_2\omega + j_3\omega^2, \ L_g = j_4 + j_5\omega, \ L_\theta = j_6 + j_7\omega, \qquad (29)$$

where $j_1, j_2, j_3, \ldots, j_7$ are called the arbitrary constants.

The zeroth order deformation problems are

$$(1 - X)L_f\left(f(\omega; X) - f_0(\omega)\right) = X\hbar_f N_f(f(\omega; X), g(\omega; X)), \qquad (30)$$

$$(1 - X)L_g\left(g(\omega; X) - g_0(\omega)\right) = X\hbar_g N_g(g(\omega; X), f(\omega; X)), \qquad (31)$$

$$\frac{k_{nf}}{k_f}T_d\theta'^2 + \frac{Br}{Re}\frac{1}{(1-\varphi)^{2.5}}\left\{A\left(g'^2 + f''^2\right) + 12f'^2\right\} + ABrHa\left(g^2 + f'^2\right). \qquad (23)$$

The Bejan number is defined as

$$Be = \frac{\frac{k_{nf}}{T_f}\left(\frac{\partial T}{\partial y}\right)^2}{\left[\begin{array}{c}\frac{k_{nf}}{T_f^2}\left(\frac{\partial T}{\partial y}\right)^2 + \frac{\mu_{nf}}{T_f}\left\{2\left(\frac{\partial u}{\partial r}\right)^2 + \frac{2}{r}(u)^2 + 2\left(\frac{\partial w}{\partial z}\right)^2 + \\ \left(\frac{\partial v}{\partial z}\right)^2 + \left(\frac{\partial w}{\partial r} + \frac{\partial u}{\partial z}\right)^2 + r\frac{\partial}{\partial r}\left(\frac{v}{r}\right)^2\right\} + \frac{\sigma_{nf}B_0^2}{T_f}\left(u^2 + v^2\right)\end{array}\right]}. \qquad (24)$$

$$(1 - X)L_\theta(\theta(\omega; X) - \theta_0(\omega)) = X\hbar_\theta N_\theta(\theta(\omega; X), f(\omega; X), g(\omega; X)), \qquad (32)$$

$$f(0; X) = 0, \ f'(0; X) = A_1, \ f'(1; X) = A_2,$$
$$g(0; X) = 1, \ g(1; X) = \gamma, \ \theta(0; X) = 1, \ \theta(1; X) = 0, \qquad (33)$$

$$N_f(f(\omega; X), g(\omega; X)) = \frac{1}{(1-\varphi)^{2.5}\left(1 - \varphi + \frac{\rho_s}{\rho_f}\varphi\right)}\frac{\partial^3 f(\omega; X)}{\partial \omega^3}$$
$$- Re\left(\frac{\partial f(\omega; X)}{\partial \omega}\right)^2 + 2Re f(\omega; X)\frac{\partial^2 f(\omega; X)}{\partial \omega^2}$$
$$+ Re(g(\omega; X))^2 - \frac{\sigma_{nf}}{\sigma_f}\frac{ReHa}{\left(1 - \varphi + \frac{\rho_s}{\rho_f}\varphi\right)}\frac{\partial f(\omega; X)}{\partial \omega}$$
$$- \frac{Re\lambda}{(1-\varphi)^{2.5}\left(1 - \varphi + \frac{\rho_s}{\rho_f}\varphi\right)}\frac{\partial f(\omega; X)}{\partial \omega}$$
$$- Re F\left(\frac{\partial f(\omega; X)}{\partial \omega}\right)^2, \qquad (34)$$

$$N_g(g(\omega; X), f(\omega; X)) = \frac{1}{(1-\varphi)^{2.5}\left(1 - \varphi + \frac{\rho_s}{\rho_f}\varphi\right)}\frac{\partial^2 g(\omega; X)}{\partial \omega^2}$$
$$- Re\left(\frac{\partial f(\omega; X)}{\partial \omega}\right)^2 + 2Re f(\omega; X)\frac{\partial g(\omega; X)}{\partial \omega}$$
$$- 2Re g(\omega; X)\frac{\partial f(\omega; X)}{\partial \omega}$$
$$- \frac{\sigma_{nf}}{\sigma_f}\frac{ReHa}{\left(1 - \varphi + \frac{\rho_s}{\rho_f}\varphi\right)}g(\omega; X), \qquad (35)$$

$$N_\theta(\theta(\omega;X), g(\omega;X), f(\omega;X)) = \frac{(k_s + 2k_f) - 2\varphi(k_f - k_s)}{(k_s + 2k_f) + \varphi(k_f - k_s)} \frac{\partial^2\theta(\omega;X)}{\partial\omega^2} + \frac{2RePr}{\left(1 - \varphi + \frac{(\rho c_p)_s}{(\rho c_p)_f}\varphi\right)} f(\omega;X) \frac{\partial\theta(\omega;X)}{\partial\omega} + \frac{Br}{(1-\varphi)^{2.5}}$$

$$\times \left(\left(\frac{\partial^2 f(\omega;X)}{\partial\omega^2}\right)^2 + \left(\frac{\partial g(\omega;X)}{\partial\omega}\right)^2 + \frac{12}{A}\left(\frac{\partial f(\omega;X)}{\partial\omega}\right)^2\right) + ReMBr\left(\left(\frac{\partial f(\omega;X)}{\partial\omega}\right)^2 + (g(\omega;X))^2\right)$$

$$+ RePr\beta\theta(\omega;X), \tag{36}$$

where $X \in [0,1]$ is the entrenching factor.

The mth order deformation problems are

$$L_f(f_m(\omega) - \chi_m f_{m-1}(\omega)) = \hbar_f R_{f,m}(\omega), \tag{37}$$

$$L_g(g_m(\omega) - \chi_m g_{m-1}(\omega)) = \hbar_g R_{g,m}(\omega), \tag{38}$$

$$L_\theta(\theta_m(\omega) - \chi_m\theta_{m-1}(\omega)) = \hbar_\theta R_{\theta,m}(\omega), \tag{39}$$

$$f_m(0) = f'_m(0) = f'_m(1) = g_m(0) = g_m(1) = \theta_m(0) = \theta_m(1) = 0, \tag{40}$$

$$R_{f,m}(\omega) = \frac{1}{(1-\varphi)^{2.5}\left(1 - \varphi + \frac{\rho_s}{\rho_f}\varphi\right)} f'''_{m-1} - Re(f'_{m-1})^2$$

$$+ 2Re\sum_{k=0}^{m-1}(f_{m-1-k}f''_k) + Re(g_{m-1})^2 - \frac{\sigma_{nf}}{\sigma_f}$$

$$\times \frac{ReHa}{\left(1 - \varphi + \frac{\rho_s}{\rho_f}\varphi\right)} f'_{m-1} - \frac{Re\lambda}{(1-\varphi)^{2.5}\left(1 - \varphi + \frac{\rho_s}{\rho_f}\varphi\right)} f'_{m-1}$$

$$- ReF(f'_{m-1})^2, \tag{41}$$

$$R_{g,m}(\omega) = \frac{1}{(1-\varphi)^{2.5}\left(1 - \varphi + \frac{\rho_s}{\rho_f}\varphi\right)} g''_{m-1} - Re(f'_{m-1})^2$$

$$+ 2Re\sum_{m=1}^{k-1}(f_{m-1-k}g'_k) - 2Re\sum_{m=1}^{k-1}(g_{m-1-k}f'_k)$$

$$- \frac{\sigma_{nf}}{\sigma_f}\frac{ReHa}{\left(1 - \varphi + \frac{\rho_s}{\rho_f}\varphi\right)} g_{k-1}, \tag{42}$$

$$R_{\theta,m}(\omega) = \frac{(k_s + 2k_f) - 2\varphi(k_f - k_s)}{(k_s + 2k_f) + \varphi(k_f - k_s)} \theta''_{k-1}$$

$$+ \frac{2RePr}{\left(1 - \varphi + \frac{(\rho c_p)_s}{(\rho c_p)_f}\varphi\right)}\sum_{m=1}^{k-1}(f_{m-1-k}\theta_k)$$

$$+ \frac{Br}{(1-\varphi)^{2.5}}\left((f''_{k-1})^2 + (g'_{k-1})^2 + \frac{12}{A}(f'_{k-1})^2\right)$$

$$+ ReMBr\left((f'_{k-1})^2 + (g_{k-1})^2\right) + RePr\beta\theta_{k-1}, \tag{43}$$

$$\chi_m = \begin{cases} 1, & m > 1 \\ 0, & m \le 1. \end{cases} \tag{44}$$

VI. RESULTS AND DISCUSSION

This section enlightens the graphical consequences of influential factors on velocity components {radial $[f'(\omega)]$, tangential $[g(\omega)]$}, temperature, entropy optimization, and Bejan number fields of the nanofluid flows between two rotating disks. In addition, the variations in skin friction and Nusselt number due to these factors are accessible through tables. The red line represents the Cu–water nanofluid, and the blue dashed line indicates the Ag–water nanofluid.

Figures 2–4 exhibit the variation in velocity components and thermal profiles via the Reynolds number. The radial velocity component escalates, while the tangential velocity component and temperature profiles have opposite behavior for the increasing Reynolds number. Actually, escalating the Reynolds number escalates viscous effects, which heighten the velocity profile along the radial direction, while deescalate the velocity profile along the tangential direction. The Reynolds number depicts the fluid viscosity. So, increasing the Reynolds number declines the fluid viscosity and hence reduces the thermal field of both nanofluids. Figures 5–7 show the effect of the nanoparticle volume fraction on the axial velocity, radial velocity, and thermal profiles. It is concluded from Figs. 5–7 that the velocity fields reduce, while the thermal profile escalates with the higher values of the nanoparticle volume fraction. The nanofluid flow variation via the Hartmann number is displayed in Figs. 8–10. The radial and tangential velocity components decline with the escalation in the Hartmann number. This effect is due to the Lorentz
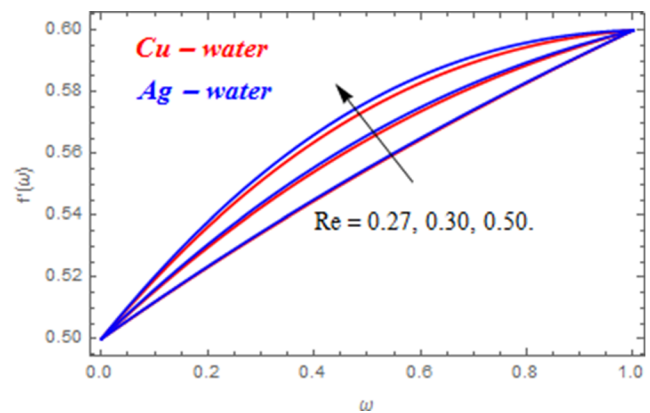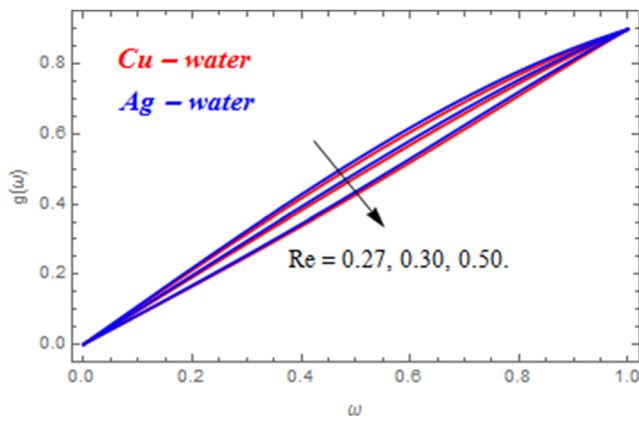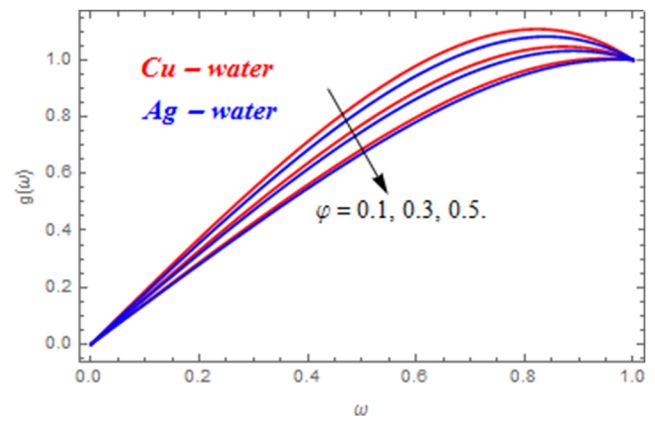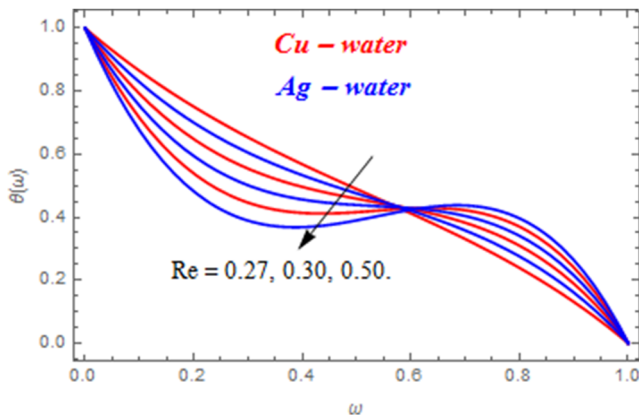

FIG. 2. Re on $f'(\omega)$.

FIG. 3. Re on $g(\omega)$.

FIG. 6. φ on $g(\omega)$.

FIG. 4. Re on $\theta(\omega)$.

FIG. 7. φ on $\theta(\omega)$.
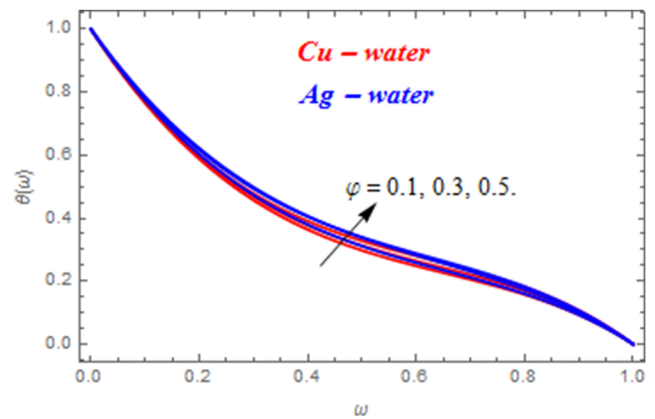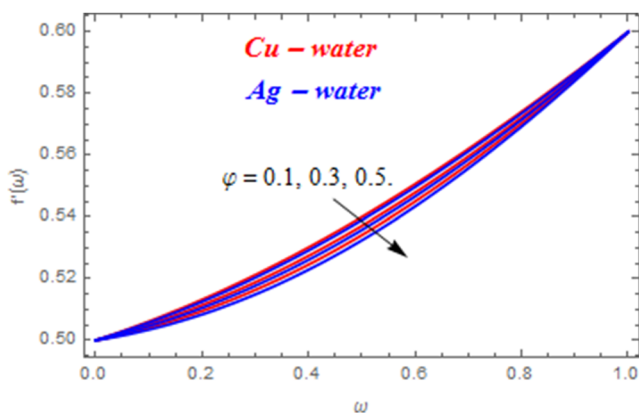
FIG. 5. φ on $f'(\omega)$.
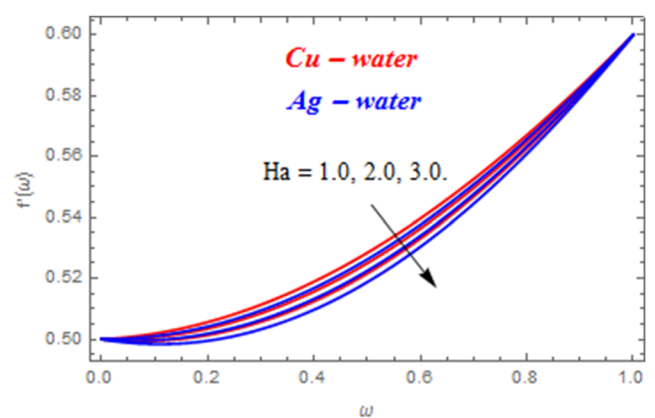
FIG. 8. Ha on $f'(\omega)$.
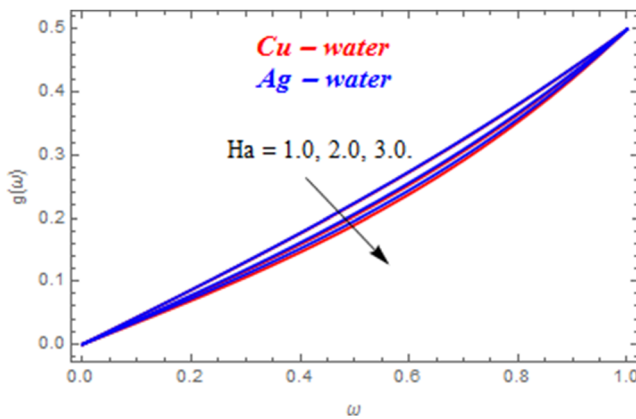
FIG. 9. *Ha* on $g(\omega)$.
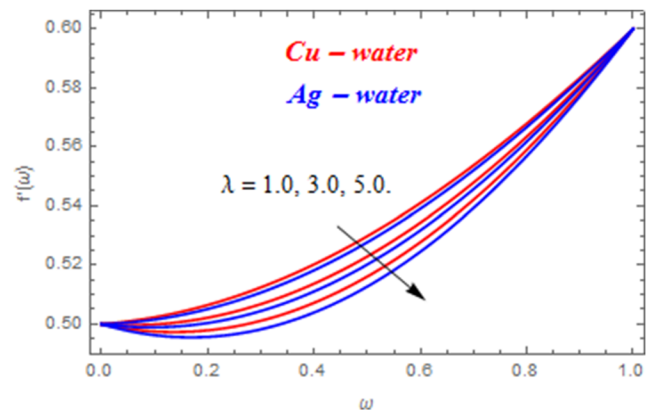
FIG. 11. Variation in $f'(\omega)$ via λ.

force, which generates the opposing force to the nanofluid flow. This force reduces the nanofluid velocity in both directions. The opposite variation is depicted against the temperature profile. In fact, the magnetic field strength increases with the increasing Hartmann number, which supplies extra heat to the nanofluid flows. Thus, the thermal field upsurges. Figure 11 presents the influence of the porosity parameter on the axial velocity component. The porous medium shows reducing behavior to the nanofluid flows. The variation in the axial velocity component via the inertial coefficient is displayed in Fig. 12. A declining impact of the inertial coefficient against the axial velocity is observed here. Figures 13 and 14 indicate the variation in nanofluid flows along the radial direction via stretching parameters. As we heighten the stretching rates of the parameters, the velocity of the nanofluid flows escalates. Thus, the heightening impact on the radial velocity component is observed via the stretching parameter. Figures 15 and 16 indicate the variation in nanofluid flows along radial and tangential directions via the rotation parameter. As we heighten the rotation parameter, the velocity of the nanofluid flows escalates. Thus, the heightening impacts on
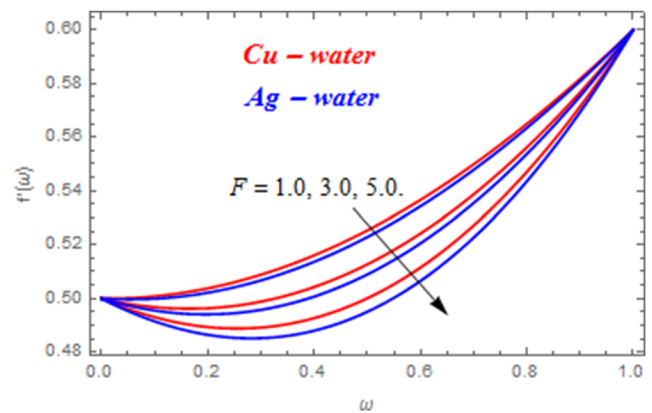
FIG. 12. Variation in $f'(\omega)$ via *F*.
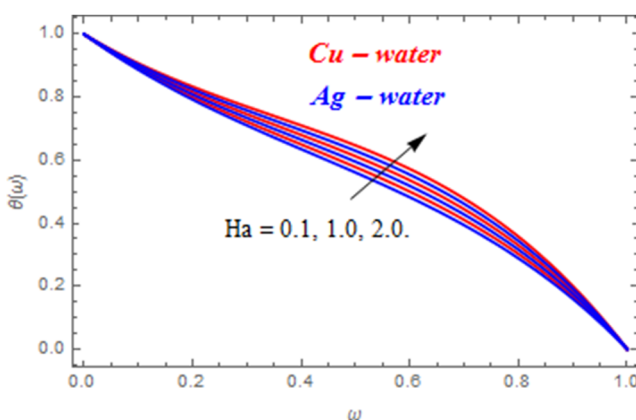
FIG. 10. *Ha* on $\theta(\omega)$.
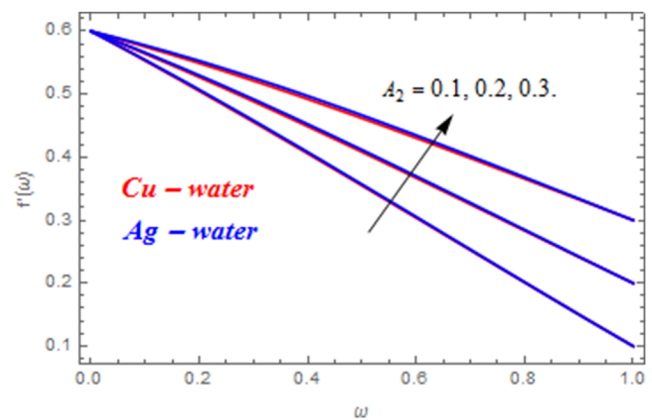
FIG. 13. A_2 on $f'(\omega)$.
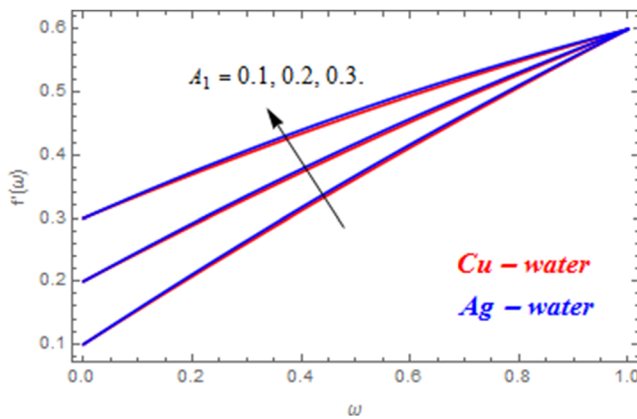
FIG. 14. A_1 on $f'(\omega)$.
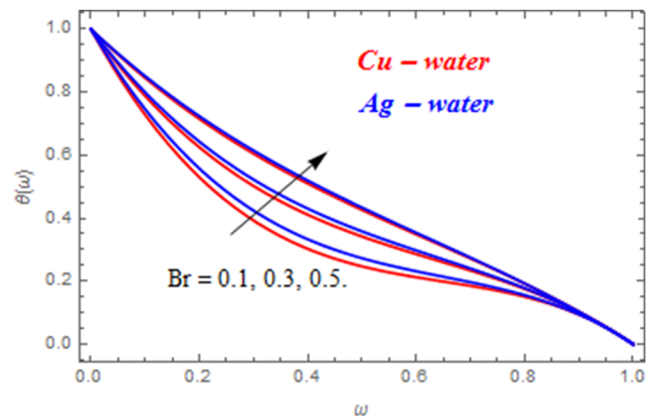
FIG. 17. Variation in $\theta(\omega)$ via Br.

FIG. 15. γ on $f'(\omega)$.
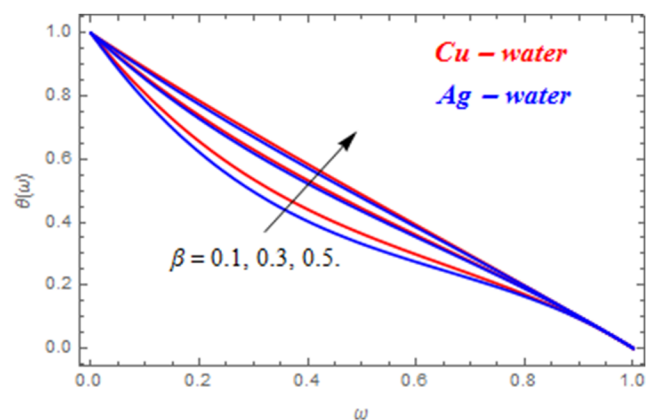
both radial and tangential velocity components are observed via the rotation parameter. Figure 17 displays the change in the thermal field due to a greater Brinkman number. Actually, the greater Brinkman number provides thermal conduction to the flow in a very small amount. Thus, the greater Brinkman number heightens the thermal field. Figure 18 indicates the effect of the heat generation factor on the thermal profile of the nanofluid flows. Higher values of the heat generation parameter produce nanofluid flows, which escalate the temperature field. The influence of the increasing Brinkman number on entropy optimization and Bejan number is demonstrated in Figs. 19 and 20. An escalating behavior of entropy generation is depicted via a higher Brinkman number. Actually, greater values of the Brinkman number reduce the thermal conduction in nanofluids, and thus, the entropy optimization is improved. A conflicting variation in the Bejan number is observed. The influence of the nanoparticle volume fraction on entropy optimization and Bejan number is exhibited in Figs. 21 and 22. Both profiles are intensifying with escalating values of the nanoparticle volume fraction. In fact, the irreversibility process increases because of fluid friction. Thus,

FIG. 16. γ on $g(\omega)$.

FIG. 18. Variation in $\theta(\omega)$ via β.
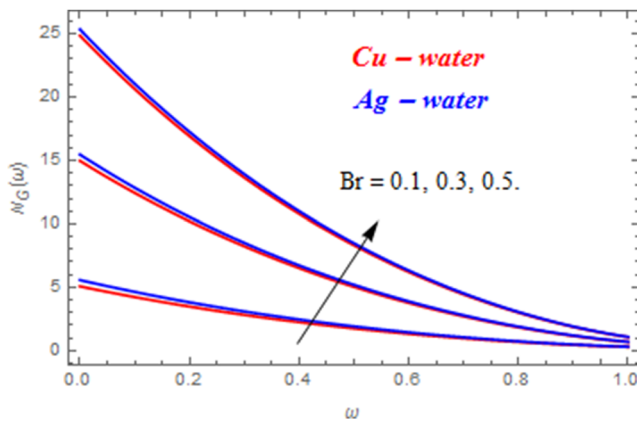
FIG. 19. *Br* on $N_G(\omega)$.

FIG. 22. φ on $Be(\omega)$.
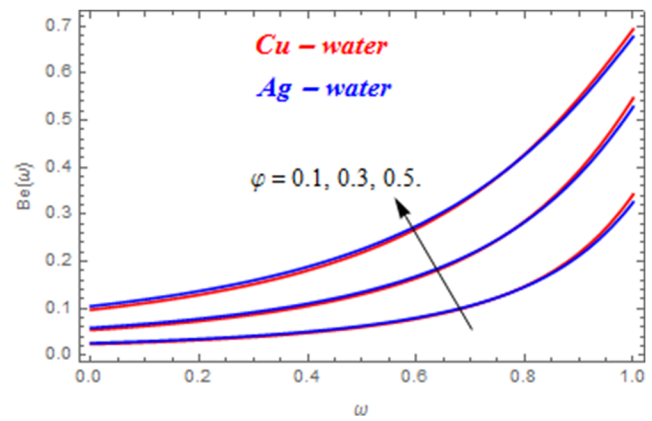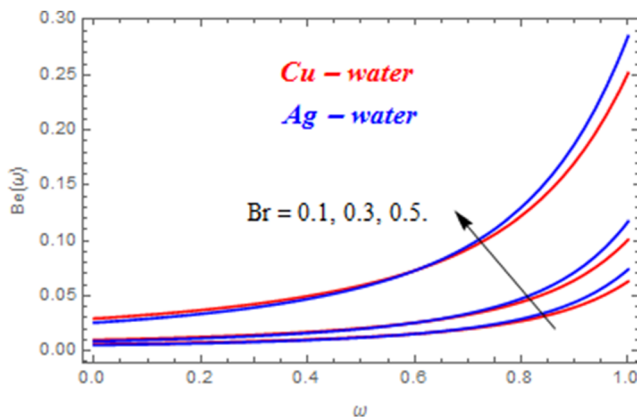
FIG. 20. *Br* on $Be(\omega)$.
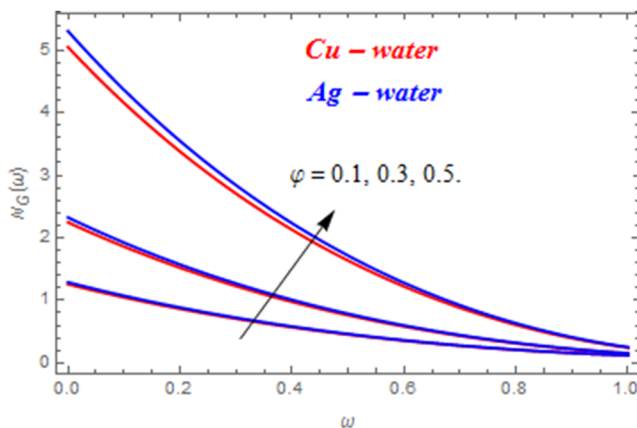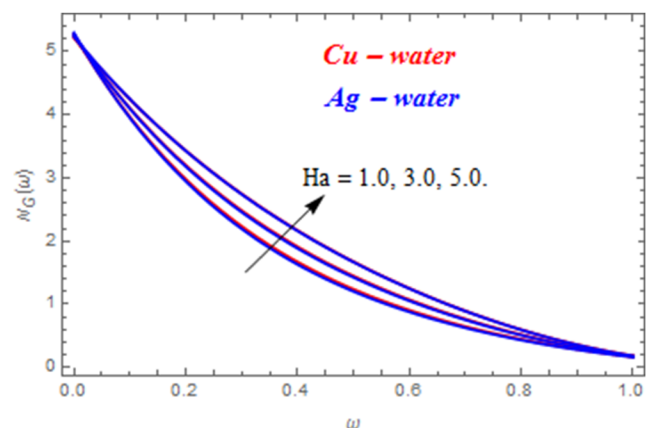
both fields are increased. The change in entropy optimization and Bejan number due to the influential Hartmann number is displayed in Figs. 23 and 24. The intensifying values of the Hartmann number surge the entropy generation, while the opposite behavior on the Bejan number is perceived. Actually, the heightening Hartmann number creates the resistive force to the motion of the nanoparticles of the nanofluids. Thus, entropy generation is increased, while the Bejan number is reduced. The influence of temperature difference on entropy optimization and Bejan number is portrayed in Figs. 25 and 26. Both profiles are increased via temperature difference. Figures 27–29 and Table I express the association of the HAM and shooting techniques. From Figs. 27–29 and Table I, it is found that both the techniques are quite applicable to the modeled problem of the nanofluids. Table II shows the thermo-physical properties of the base fluid and nanoparticles. Table III is displayed in order to analyze the impact of embedded factors on drag force. A higher Reynolds number escalates the skin friction at the lower disk, while deescalates the skin friction at the upper disk for the Ag–water nanofluid. In addition, the increasing behavior is depicted at both

FIG. 21. φ on $N_G(\omega)$.

FIG. 23. *Ha* on $N_G(\omega)$.
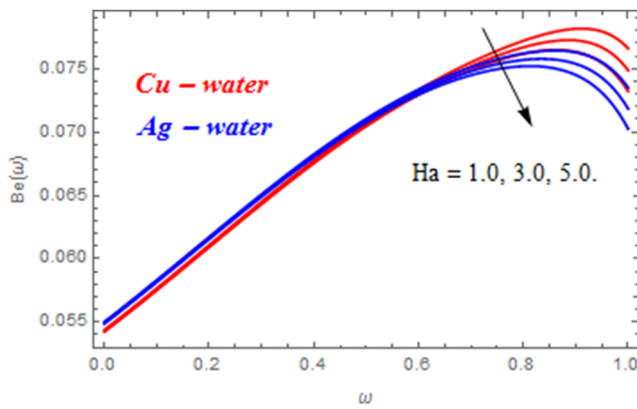
FIG. 24. Ha on $Be(\omega)$.
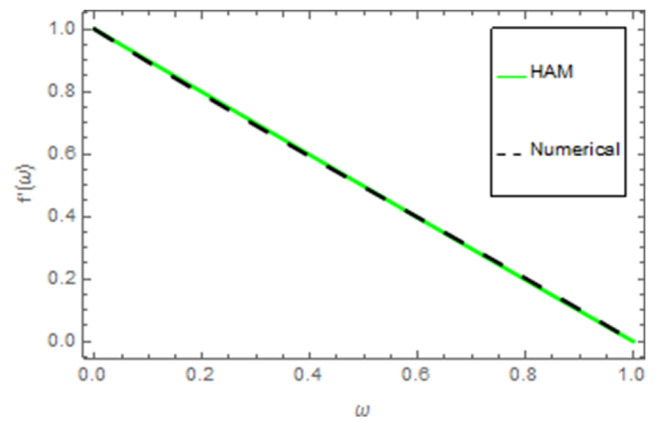
FIG. 27. HAM vs shooting for $f'(\omega)$.
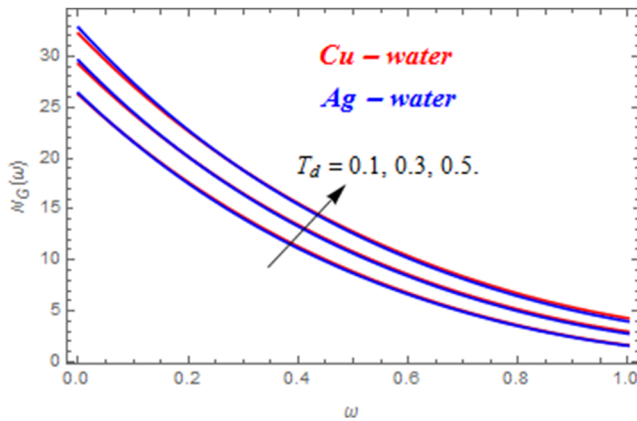
FIG. 25. T_d on $N_G(\omega)$.
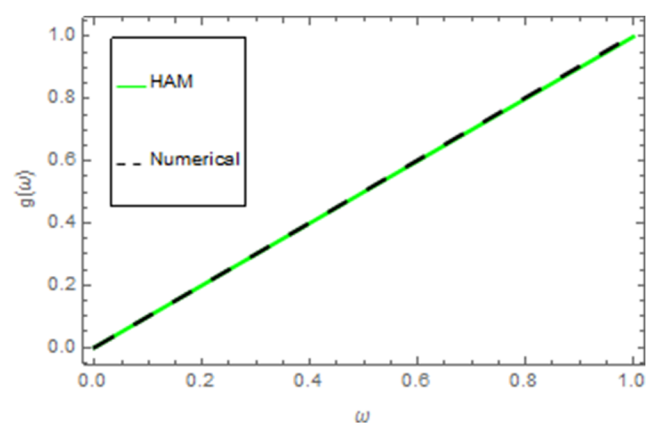
FIG. 28. HAM vs shooting for $g(\omega)$.
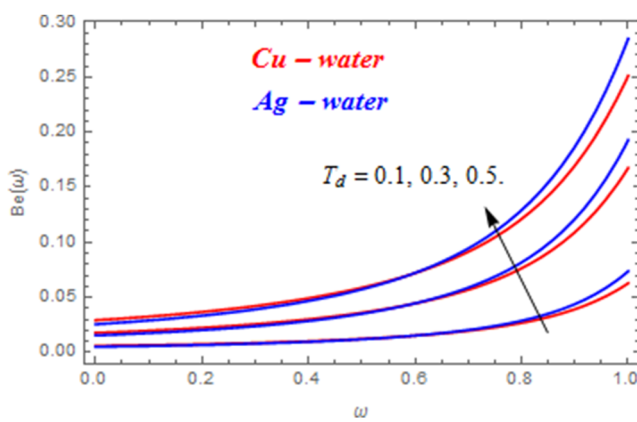
FIG. 26. T_d on $Be(\omega)$.
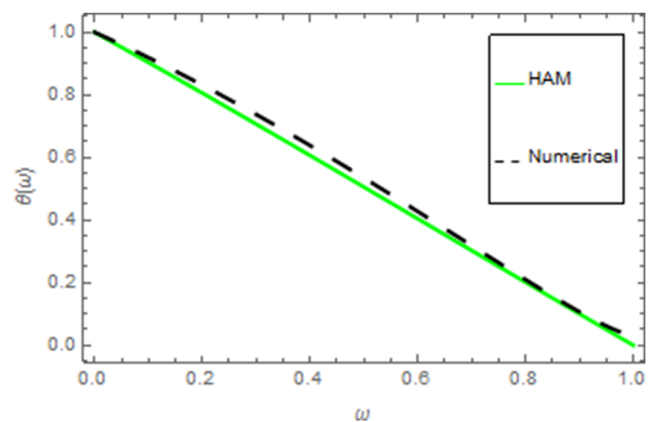
FIG. 29. HAM vs shooting for $\theta(\omega)$.

TABLE I. Association between shooting and HAM for $f'(\omega)$, $g(\omega)$, and $\theta(\omega)$.

| | $f'(\omega)$ | | $g(\omega)$ | | $\theta(\omega)$ | |
ω	HAM	Shooting	HAM	Shooting	HAM	Shooting
0.0	0.000 000	0.000 000	0.000 000	-5.3455×10^{-10}	1.000 000	1.000 000
0.2	0.179 837	0.178 984	0.200 278	0.200 744	0.805 720	0.827 635
0.4	0.319 366	0.317 233	0.400 529	0.401 781	0.606 375	0.630 152
0.6	0.418 674	0.416 121	0.600 672	0.600 672	0.404 148	0.414 028
0.8	0.477 971	0.476 095	0.800 563	0.800 563	0.201 267	0.190 028
1.0	0.497 621	0.496 460	1.000 000	1.005 020	5.1499×10^{-18}	0.004 763

TABLE II. Thermo-physical properties of base fluids and nanoparticles.

	ρ (kg/m^3)	c_p (J/kg K)	k (W/m K)	σ (1/γm)
Silver (Ag)	10 500	235	429	6.30×10^7
Copper (Cu)	8933	385	401	5.96×10^7
Water (H$_2$O)	997.1	4179	0.613	0.05

disks for the Cu–water nanofluid. A similar impact is also observed for both nanofluids for a higher Hartmann number. At the lower disk surface, with higher values of the porosity parameter, Ag–water and Cu–water nanofluids escalate, whereas conflicting conduct is depicted at the upper disk for both nanofluids. The greater values of the inertial coefficient escalate both nanofluids at the lower disk surface, while conflicting behavior is depicted at the upper disk for both nanofluids. The escalating stretching rates decline the surface drag

TABLE III. Numerical consequences of the surface drag force at the lower disk (C_{f0}) and upper disk (C_{f1}) for both nanofluids.

| | | | | | | | | Ag–water | | Cu–water | |
Re	Ha	λ	F	A_1	A_2	γ	φ	C_{f0}	C_{f1}	C_{f0}	C_{f1}
0.1	0.3	0.5	0.1	0.7	0.5	0.8	0.1	0.5804	0.3966	0.5836	0.3995
0.2								0.7116	0.3497	0.6966	0.3498
0.3								0.8348	0.2851	0.8116	0.3372
0.4	0.1							0.9066	0.3767	0.8747	0.3634
	0.2							0.9317	0.3746	0.8992	0.3596
	0.3							0.9568	0.3742	0.9257	0.3577
	0.4	0.1						0.9420	0.4139	0.9094	0.3996
		0.2						0.9457	0.4037	0.9131	0.3889
		0.3						0.9480	0.3937	0.9171	0.3783
		0.4	0.2					0.9509	0.3663	0.9299	0.3499
			0.3					0.9652	0.3586	0.9390	0.3425
			0.4					0.9696	0.3511	0.9485	0.3351
			0.5	0.1				0.9398	0.4745	0.9926	0.4877
				0.3				0.8673	0.2928	0.8381	0.2925
				0.5				0.8108	0.2527	0.7804	0.2280
				0.7	0.1			1.1671	0.8985	1.1521	0.8949
					0.4			0.9890	0.4849	0.9620	0.4753
					0.6			0.9412	0.3192	0.9066	0.2935
					0.5	0.3		1.9930	0.9792	1.9967	0.9563
						0.5		1.9286	1.1043	1.8713	1.1361
						0.7		1.8664	1.2120	1.7768	1.2971
						0.8	0.20	2.5818	1.4261	2.6059	1.3951
							0.21	2.6243	1.4751	2.6499	1.4411
							0.22	2.6682	1.5241	2.6951	1.4891

TABLE IV. Numerical results for the thermal transfer rate at the lower disk (Nu_{x0}) and upper disk (Nu_{x1}) for both nanofluids when $A_1 = 0.7$, $A_2 = 0.5$, Re = 0.4, and $\gamma = 0.8$.

					Ag–water		Cu–water	
Ha	λ	F	Ec	φ	Nu_{x0}	Nu_{x1}	Nu_{x0}	Nu_{x1}
0.1	0.5	0.1	0.7	0.1	2.2586	0.9931	2.1600	0.9694
0.2					2.2282	0.9968	2.1405	0.9830
0.3					2.1080	0.9992	2.1201	0.9964
0.3	0.1				2.2127	0.9936	2.2250	0.9896
	0.2				2.2115	0.9952	2.2238	0.9913
	0.3				2.2003	0.9969	2.2225	0.9931
	0.5	0.2			2.1800	0.9117	2.2191	0.9978
		0.3			2.1759	0.9132	2.2181	0.9992
		0.4			2.1649	0.9146	2.2172	1.0014
		0.1	0.2		2.0511	0.9452	2.1629	2.1214
			0.3		1.5071	2.2205	1.5094	2.2250
			0.4		1.3974	2.3204	1.3998	2.3248
			0.1	0.20	1.9948	2.4545	1.9989	2.4635
				0.21	2.1479	2.5041	2.1522	2.5135
				0.22	2.1921	2.5549	2.1966	2.5648

force of both nanofluids at both disks. The rising rotation factors reduce the surface drag force for both nanofluids at the lower disk, while the reverse impression is observed at the upper disk. The skin friction rises for both nanofluids at both disks with escalating values of the nanoparticle volume fraction. Table IV displays the variation in the Nusselt number via influential factors. The Nusselt number escalates with higher values of the Hartmann number and inertial coefficient at the lower disk for both nanofluids, while reduces at the upper disk for both nanofluids. The escalating values of the porosity parameter reduce Nu at the lower disk, while escalate Nu at the upper disk for both nanofluids. The rising estimations of the Eckert number decline Nu at the lower disk, while the opposing performance is observed at the upper disk for both nanofluids. The growing values of the nanoparticle volume fraction escalate Nu at both disks for both nanofluids.

VII. CONCLUSION

Entropy generation in Darcy–Forchheimer flows of Cu–water and Ag–water nanofluids between two rotating disks is investigated. A magnetic field along radial and tangential directions is applied. The modeled coupled equations are solved analytically and numerically. Core points of the present analysis for both nanofluids are as follows:

a. The radial velocity component is heightened, while the tangential velocity component and temperature profile are reduced with the Reynolds number.

b. The radial and tangential velocity components are declined, while the temperature profile is escalated with the Hartmann number and nanoparticle volume fraction.

c. The radial velocity component is declined with the porosity parameter and inertial coefficient, while heightened with stretching parameters.

d. The radial and tangential velocity components are escalated with the rotation parameter.

e. The temperature profile is escalated with the Brinkman number and heat generation parameter.

f. Entropy generation and Bejan number are increased with the volume fraction of nanoparticles, temperature difference, and Brinkman number.

g. The entropy generation is improved with the Hartmann number, while the Bejan number is reduced with the Hartmann number.

h. The close contract of both analytical and numerical techniques is observed.

DATA AVAILABILITY

The data that support the findings of this study are available from the corresponding author upon reasonable request.

REFERENCES

[1] S. U. S. Choi, "Enhancing thermal conductivity of fluids with nanoparticles," in *ASME International Mechanical Engineering Congress and Exposition* (ASME, 1995), Vol. 66, pp. 99–105.

[2] K. S. Hwang, S. P. Jang, and S. U. S. Choi, "Flow and convective heat transfer characteristics of water-based Al_2O_3 nanofluids in fully developed laminar flow regime," Int. J. Heat Mass Transfer **52**, 193–199 (2009).

[3] M. M. Bhatti and M. M. Rashidi, "Effects of thermo-diffusion and thermal radiation on Williamson nanofluid over a porous shrinking/stretching sheet," J. Mol. Liq. **221**, 567–573 (2016).

[4] M. Hatami, S. A. R. Sahebi, A. Majidian, M. Sheikholeslami, D. Jing, and G. Domairry, "Numerical analysis of nanofluid flow conveying nanoparticles through expanding and contracting gaps between permeable walls," J. Mol. Liq. **212**, 785–791 (2015).

[5] T. Hayat, S. Qayyum, M. Imtiaz, and A. Alsaedi, "Comparative study of silver and copper water nanofluids with mixed convection and nonlinear thermal radiation," Int. J. Heat Mass Transfer **102**, 723–732 (2016).

[6] N. S. Akbar, M. Raza, and R. Ellahi, "Copper oxide nanoparticles analysis with water as base fluid for peristaltic flow in permeable tube with heat transfer," Comput. Methods Progr. Biomed. **130**, 22–30 (2016).

[7] R. Ellahi, M. Hassan, and A. Zeeshan, "Shape effects of nanosize particles in image nanofluid on entropy generation," Int. J. Heat Mass Transfer **81**, 449–456 (2015).

[8] M. Sheikholeslami and R. Ellahi, "Three dimensional mesoscopic simulation of magnetic field effect on natural convection of nanofluid," Int. J. Heat Mass Transfer **89**, 799–808 (2015).

[9] T. Hayat, A. Aziz, T. Muhammad, and A. Alsaedi, "On magnetohydrodynamic three dimensional flow of nanofluid over a convectively heated nonlinear stretching surface," Int. J. Heat Mass Transfer **100**, 566–572 (2016).

[10] F. M. Abbasi, S. A. Shehzad, T. Hayat, and B. Ahmad, "Doubly stratified mixed convection flow of Maxwell nanofluid with heat generation/absorption," J. Magn. Magn. Mater. **404**, 159–165 (2016).

[11] C. S. K. Raju, N. Sandeep, and V. Sugunamma, "Unsteady magneto-nanofluid flow caused by a rotating cone with temperature dependent viscosity: A surgical implant application," J. Mol. Liq. **222**, 1183–1191 (2016).

[12] M. Jonnadula, P. Polarapu, M. G. Reddy, and M. Venkateswarlu, "Influence of thermal radiation and chemical reaction in MHD flow, heat and mass transfer over a stretching surface," J. Chem. Eng. Process. **127**, 1315–1322 (2015).

[13] R. Ellahi, "The effects of MHD and temperature dependent viscosity on the flow of non-Newtonian nanofluid in a pipe: Analytical solutions," Appl. Math. Model. **37**, 1451–1467 (2013).

[14] P. Kumam, Z. Shah, A. Dawar, H. U. Rasheed, and S. Islam, "Entropy generation in MHD radiative flow of CNTs Casson nanofluid in rotating channels with heat source/sink," Math. Probl Eng. **2019**, 9158093.

[15] S. O. Alharbi, A. Dawar, Z. Shah, W. Khan, M. Idrees, S. Islam, and I. Khan, "Entropy generation in MHD Eyring–Powell fluid flow over an unsteady oscillatory porous stretching surface under the impact of thermal radiation and heat source/sink," Appl. Sci. **8**, 2588 (2018).

[16] A. Khan, Z. Shah, S. Islam, A. Dawar, E. Bonyah, H. Ullah, and A. Khan, "Darcy–Forchheimer flow of MHD CNTs nanofluid radiative thermal behaviour and convective non uniform heat source/sink in the rotating frame with microstructure and inertial characteristics," AIP Adv. **8**, 125024 (2018).

[17] Z. Shah, P. Kumam, A. Dawar, E. O. Alzahrani, and P. Thounthong, "Study of the couple stress convective micropolar fluid flow in a Hall MHD generator system," Front. Phys. **7**, 171 (2019).

[18] M. Turkyilmazoglu, "An asymptotic investigation into the stabilization effect of suction in the rotating-disk boundary layer flow," Comput. Math. Appl. **53**, 750–759 (2007).

[19] M. Hatami, M. Sheikholeslami, and D. D. Ganji, "Laminar flow and heat transfer of nanofluid between contracting and rotating disks by least square method," Powder Technol. **253**, 769–779 (2014).

[20] W. M. Yan and C. Y. Soong, "Mixed convection flow and heat transfer between two co-rotating porous disks with wall transpiration," Int. J. Heat Mass Transfer **40**, 773–784 (1997).

[21] L. H. You, Y. Y. Tang, J. J. Zhang, and C. Y. Zheng, "Numerical analysis of elastic-plastic rotating disks with arbitrary variable thickness and density," Int. J. Solid Struct. **37**, 7809–7820 (2000).

[22] C. Y. Soong, "Theoretical analysis for axisymmetric mixed convection between rotating coaxial disks," Int. J. Heat Mass Tran. **39**, 1569–1583 (1996).

[23] T. Hayat, M. Imtiaz, A. Alsaedi, and F. Alzahrani, "Effects of homogeneous–heterogeneous reactions in flow of magnetite-Fe_3O_4 nanoparticles by a rotating disk," J. Mol. Liq. **216**, 845–855 (2016).

[24] N. A. Alreshidi, Z. Shah, A. Dawar, P. Kumam, M. Shutaywi, and W. Watthayu, "Brownian motion and thermophoresis effects on MHD three dimensional nanofluid flow with slip conditions and Joule dissipation due to porous rotating disk," Molecules **25**, 729 (2020).

[25] A. Bejan, "A study of entropy generation in fundamentsl convective heat transfer," J. Heat Tran. **101**, 718–725 (1979).

[26] T. Hayat, L. Sajjad, M. I. Khan, M. I. Khan, and A. Alsaedi, "Salient aspects of thermodiffusion and diffusion thermo on unsteady dissipative flow with entropy generation," J. Mol. Liq. **282**, 557–565 (2019).

[27] A. Dawar, Z. Shah, W. Khan, M. Idrees, and S. Islam, "Unsteady squeezing flow of magnetohydrodynamic carbon nanotube nanofluid in rotating channels with entropy generation and viscous dissipation," Adv. Mech. Eng. **11**(1), 1–18 (2019).

[28] M. Govindaraju, N. V. Ganesh, B. Ganga, and A. K. A. Hakeem, "Entropy generation analysis of magneto hydrodynamic flow of a nanofluid over a stretching sheet," J. Egypt. Math. Soc. **23**, 429–434 (2015).

[29] M. I. Khan, T. Hayat, M. I. Khan, M. Waqas, and A. Alsaedi, "Numerical simulation of hydromagnetic mixed convective radiative slip flow with variable fluid properties: A mathematical model for entropy generation," J. Phys. Chem. Solids **125**, 153–164 (2019).

[30] N. V. Ganesh, Q. M. Al-Mdallal, and A. J. Chamkha, "A numerical investigation of Newtonian fluid flow with buoyancy, thermal slip of order two and entropy generation," Case Stud. Therm. Eng. **13**, 100376 (2019).

[31] T. Hayat, S. Farooq, B. Ahmad, and A. Alsaedi, "Effectiveness of entropy generation and energy transfer on peristaltic flow of Jeffrey material with Darcy resistance," Int. J. Heat Mass Tranfer **106**, 244–252 (2017).

[32] T. Hayat, S. A. Khan, M. I. Khan, and A. Alsaedi, "Theoretical investigation of Ree–Eyring nanofluid flow with entropy optimization and Arrhenius activation energy between two rotating disks," Comput. Methods Progr. Biomed. **177**, 57–68 (2019).

[33] Z. Shah, E. O. Alzahrani, A. Dawar, W. Alghamdi, and M. Z. Ullah, "Entropy generation in MHD second-grade nanofluid thin film flow containing CNTs with Cattaneo–Christov heat flux model past an unsteady stretching sheet," Appl. Sci. **10**, 2720 (2020).

[34] F. Shah, M. I. Khan, T. Hayat, M. I. Khan, A. Alsaedi, and W. A. Khan, "Theoretical and mathematical analysis of entropy generation in fluid flow subject to aluminumand ethylene glycol nanoparticles," Comput. Methods Progr. Biomed. **182**, 105057 (2019).

[35] W. Deebani, A. Tassaddiq, Z. Shah, A. Dawar, and F. Ali, "Hall effect on radiative Casson fluid flow with chemical reaction on a rotating cone through entropy optimization," Entropy **22**, 480 (2020).

[36] K. Shah, H. Khalil, and R. A. Khan, "Analytical solutions of fractional order diffusion equations by natural transform method," Iran. J. Sci. Technol., Trans. A: Sci. **42**(3), 1479–1490 (2016).

[37] K. Shah, "Coupled systems of boundary value problems for nonlinear fractional differential equations," J. Pure Appl. Math. **2**(2), 14–17 (2018).

[38] K. Shah and M. Akram, "Numerical treatment of non-integer order partial differential equations by omitting discretization of data," Comput. Appl. Math. **37**(5), 6700–6718 (2018).

[39] S. Islam, A. Khan, W. Deebani, E. Bonyah, N. A. Alreshidi, and Z. Shah, "Influences of Hall current and radiation on MHD micropolar non-Newtonian hybrid nanofluid flow between two surfaces," AIP Adv. **10**, 055015 (2020).

[40] T. Hayat, H. Nazar, M. Imtiaz *et al.*, "Darcy–Forchheimer flows of copper and silver water nanofluids between two rotating stretchable disks," Appl. Math. Mech. **38**, 1663–1678 (2017).

[41] H. C. Brinkman, "The viscosity of concentrated suspensions and solutions," J. Chem. Phys. **20**, 571–581 (1952).

[42] R. Ellahi, M. Hassan, A. Zeeshan, and A. A. Khan, "The shape effects of nanoparticles suspended in HFE-7100 over wedge with entropy generation and mixed convection," Appl. Nanosci. **6**(5), 641–651 (2016).

[43] J. C. A. Maxwell, *Treatise on Electricity and Magnetism* (Cambridge University Press, Cambridge, 1904).

[44] T. Cebeci and P. Bradshaw, *Physical and Computational Aspects of Convective Heat Transfer* (Springer-Verlag, New York, 1988).